



PRELIMINARY ESTIMATES OF THE RHEOLOGICAL PROPERTIES OF 1984 MAUNA LOA LAVA

By Henry J. Moore

ABSTRACT

During April 2–3, 1984, the visual characteristics of the lava of Mauna Loa changed dramatically along the length of the flow that was fed from vents near 2,850-m (9,350-ft) elevation. In the upper reaches, 2,500-m (8,200-ft) elevation and 3 km from the vents, the flow was composed of sparse clinkers and cinders in a matrix of incandescent lava and was confined within a channel 20 m across. The flow appeared to be laminar and more or less steady, with a velocity of about 5.3 m/s at its center. Concentration and mean size of solid to incandescent objects carried along by the flow increased downstream. In the lower reaches, at 1,620-m (5,300-ft) elevation and 15 km from the vents, the flow looked like a slowly moving mass of debris confined within rubbly levees; the debris included warm to incandescent fragments that were block size and smaller along with molten lava and incandescent globs or clots. Movement of the flow occurred by displacement of discrete, intact units with boundaries that paralleled the crests of the rubbly levees at the margins of the flow. Flow appeared to be laminar but unsteady, with surges and ebbs. Typical flow velocities were in the range of 0.1–0.3 m/s.

Apparent viscosity of the lava on a given day increased along the length of the flow and with time at some locations. On April 2, it was about 10^2 Pa·s (10^3 poise) at the vents, 10^3 Pa·s (10^4 poise) 3 km from the vents, 10^5 Pa·s (10^6 poise) 15 km from the vents, and probably near 10^7 Pa·s (10^8 poise) at the toe of one flow. Apparent viscosity at the vents increased from about 10^2 Pa·s on April 2 to 2×10^3 Pa·s on April 13. These values compare favorably with field and laboratory data on viscosity of basalt at the same temperatures and with similar stresses and rates of shear as the Mauna Loa lava.

Rheology of the lava probably varied along the length of the flow and with time. It could have been a Newtonian fluid near the vents, a Bingham fluid 3 km from the vents, and a pseudoplastic fluid farther from the vents. Other models of fluids may also apply.

Volume flow rate in the channel at the vents on April 3 was near 1.5×10^6 – 2.0×10^6 m³/h, about 12 times larger than that 15 km from the vents. With certain assumptions, an approximation of conservation of mass along the length of the flow requires that the density of lava flowing from the vents was 220 kg/m³ and implies a mass flow rate near 0.33×10^9 – 0.44×10^9 kg/h. If these masses were deposited as lava with an average density of 2,200 kg/m³, the volume flow rate would appear to be 0.15×10^6 – 0.20×10^6 m³/h.

INTRODUCTION

This paper estimates the rheological properties of the lava during the 1984 eruption of Mauna Loa Volcano in Hawaii and

applies the results to the problems of volume and mass flow rates along the flow on one day. The derived rheological properties are based on visual observations while the flow was in progress; time and resources have permitted only partial analysis of the available data. Time-lapse photography and motion pictures of the eruption should be reviewed and analyzed in future rheological studies.

The 1984 eruption of Mauna Loa began at 0126 Hawaii standard time (H.s.t.) on March 25 and ended late on April 15 (Lockwood and others, 1984a, 1985). Initially, lava fountains issued from eruption fissures in the southwest corner of the summit caldera (Mokuaweoweo), but within a few hours eruptions from fissures migrated down the southwest rift zone, northeastward across Mokuaweoweo, and down the upper northeast rift zone (Lockwood and others, 1984b, 1985). Later on March 25, lava began pouring sequentially down the northeast rift zone from separate, isolated vents above eruption fissures. At about 1630 H.s.t. on March 25, lava was issuing from fissure vents at 2,830–2,900-m (9,300–9,500-ft) elevations that became the principal sources of lava for the remainder of the eruption (Lipman and Banks, chapter 57; fig. 58.1). Three southerly flow lobes fed by these vents stagnated by March 27, but the fourth (flow 1) was fed at a fairly constant volume flow rate ($\sim 1.5 \times 10^6$ m³/h). Large flow rates were sustained from March 30 to April 7; after April 7 flow rates declined. Flow 1 advanced rapidly as a narrow aa sheet to the 910-m (3,000-ft) level, 25 km from the vents, and a lava channel had formed within the sheet by March 29. On March 29, a breakout or channel overflow near the 1,740-m (5,700-ft) level cut off the supply of lava to flow 1 so that it moved only about another kilometer in about a day and then stopped. Lava of this breakout gave rise to flow 1A which advanced rapidly along a course subparallel to and north of flow 1; advance of flow 1A gradually decreased until April 5, when it stopped about 27 km from the vents. A series of overflows that progressed upstream beginning April 3 reduced the lava supply to flow 1A and culminated in a major breakout at the 1,980-m (6,500-ft) level around noon on April 5. This major breakout cut off the lava supply to flow 1A and produced flow 1B, which flowed toward the northeast. Repeated channel blockages and overflows continued progressively upstream from April 5 to 8. On April 7, lava production at the vent began to dwindle; subsequently the flow system stagnated and vent activity ceased.

Flow 1, initially a narrow aa sheet flow, lenticular in profile, evolved into a flow system with three zones: (1) a channel zone within the sheet flow and below the vents, (2) a transition zone, and (3) a

dispersed-flow zone led by the advancing toe (Lipman and Banks, chapter 57). On March 28, just before the breakout of flow 1A, a stable channel zone extended from the vents about 11 km down to about the 1,830-m (6,000-ft) level; the transition zone extended 10 km down to within 1 or 2 km of the toe, then at the 1,220-m (4,000-ft) level, and the dispersed-flow zone made up the remainder. By April 3, the channel zone extended down to the 1,770-m (5,800-ft) level, the transition zone of flow 1A extended 3–4 km down to the 1,580-m (5,200-ft) level, and the dispersed-flow zone extended down to the toe of flow 1A at the 1,010-m (3,300-ft) level about 26 km from the vents. Significant blockages and obstructions of flow in the channel were observed on March 29. Such blockages and obstructions, which ponded the lava, increased in size and number upstream toward the vents with time. Overflows of lava caused by the blockages and obstructions created lava dams, levees, and elevated lava ponds along the channel zone. Minor failures of blockages in the lava dams produced increased flowage from the ponds and surging and ebbing flow downstream. Larger failures in the lava dams caused larger surges of lava, which overflowed the levees and produced small flows along the channel edges. Major failures caused major surges and breakouts or overflows of large volumes of lava. Such major overflows gave rise to flow 1A on March 29 and flow 1B on April 5. Subsequently, repeated blockages and overflows occurred progressively upstream.

Lava temperature at the vents was $1,140 \pm 3^\circ\text{C}$ throughout the eruption, and that of the most fluid lava at channel stations as far as 10 km from the vents was in the range of $1,135 \pm 5^\circ\text{C}$ (Lipman and Banks, chapter 57). Reported temperatures of the most fluid lava in the channel beyond about 12 km from the vents were 1,086–1,126 $^\circ\text{C}$ (flow 1A at elevations of 1,750–1,150 m; see Lipman and Banks, chapter 57). Bulk temperatures at the various channel stations and at lower elevations may have been lower than this, because there were coherent glowing blocks and solidified fragments in the flows. Bulk density of the flowing lava varied greatly and ranged from 330–2,600 kg/m^3 (0.33–2.6 g/cm^3); density tended to increase with distance from the vents (Lipman and Banks, chapter 57). Finally, the concentration of microphenocrysts in the lava increased with time at the vents and with distance from the vents (Lipman and Banks, chapter 57).

Subsequent sections of this paper will (1) describe the author's observations; (2) discuss the flow models and equations used to estimate the rheological properties of the flows, volume flow rates, and mass flow rates; (3) present the results; (4) discuss the results; and (5) list the conclusions.

ACKNOWLEDGMENTS

Robert Decker, Scientist in Charge, and John P. Lockwood of the Hawaiian Volcano Observatory were instrumental in making arrangements for the author to witness the eruption and observe "redrock" for the very first time. Cordial hospitality and assistance were provided by the staff of the Hawaiian Volcano Observatory. Jack Lockwood, Peter Lipman, Norman Banks, and Christina

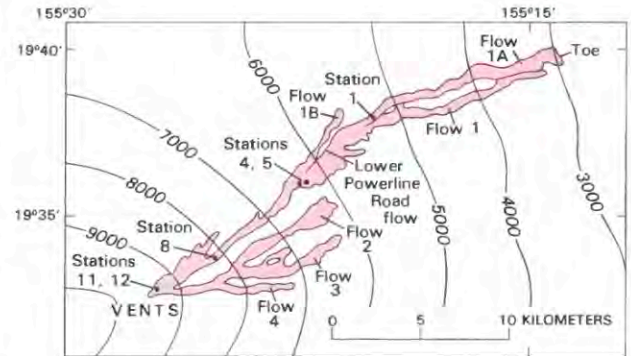


FIGURE 58.1.—Sketch map of the 1984 Mauna Loa lava flows showing stations referred to in text. Contour interval is 1,000 feet.

Neal allowed this tyro to accompany them in the field with exemplary tolerance and patience. Helicopter pilots Bill Lacey, Jr., Tom Haupman, Ed Spencer, and Ken Ellard safely delivered the author to and from flows. Work was partly funded by NASA contract W-15-462.

OBSERVATIONS

Observations of the author for three localities (fig. 58.1) along the flow for the period April 2 through April 7 are described and discussed below. These localities are (see Lipman and Banks, chapter 57): (a) station 8, vent of 1852, 2,500 m (8,200 ft), 3 km from the vents; (b) stations 4 and 5, 1,920–1,950 m (6,300–6,400 ft), about 9 km from the vents; and (c) station 1, 1,620 m (5,300 ft), about 15 km from the vents. The first two localities were in the stable channel zone, and the third in the transition zone. Also included are the author's description of an advancing, unconfined, wide flow from an overflow and Hawaiian Volcano Observatory staff reports on the toe of flow 1A. These two flows correspond to dispersed flow.

STATION 8, APRIL 2–7

The flow appeared to be a mass of cinders and clinkers imbedded in a matrix of incandescent lava estimated to be 4 m deep and confined within a channel 20 m across (fig. 58.2). A few floating silvery, meter-size blocks were carried along by the flow. Flow appeared to be laminar and nonturbulent. The central portion of the flow, about 1 m wide, moved as a plug-like unit of silvery to light gray crusty material in a matrix of incandescent lava (fig. 58.3). Between the plug-like center and the margins, bands of red incandescent lava and small cinders and clinkers were aligned parallel to the channel edges. Velocity decreased from about 5.3 m/s near the center to zero at the channel edge (fig. 58.3). The meter-size and smaller blocks did not rotate around horizontal axes and those near



FIGURE 58.2.—Lava in channel at station 8 on April 5. Channel is about 20 m wide; flow surface is composed of very light gray cinders and clinkers set in a matrix of reddish-orange lava; flow from right to left. Foreground is aa of sheet flow.

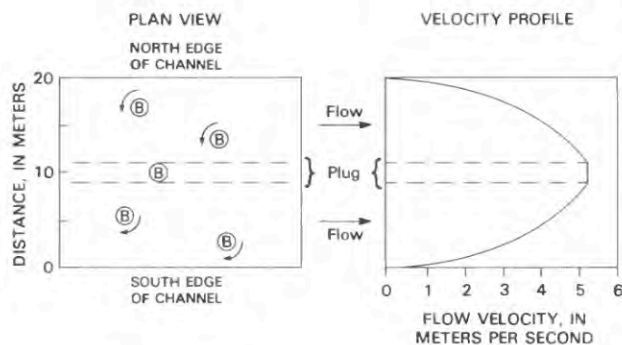


FIGURE 58.3.—Diagrammatic plan view and velocity profile for lava channel at station 8. In plan view, one-meter-wide plug moves as unit with uniform velocity. Blocks (B) north of plug rotate counterclockwise around vertical axes; blocks south of plug rotate clockwise around vertical axes; blocks in plug do not rotate. Velocity profile shows velocity of lava increases smoothly from zero at channel edge to 5.3 m/s in the plug.

the center did not rotate around vertical axes. Between the center and the margin, the blocks rotated around vertical axes. Rotation was counterclockwise on the north side of the channel and clockwise on the south side; the lava was moving from the west toward the east. The flow was remarkably quiet, but it did make faint shushing and swishing sounds. Volume flow rates obtained by multiplying the

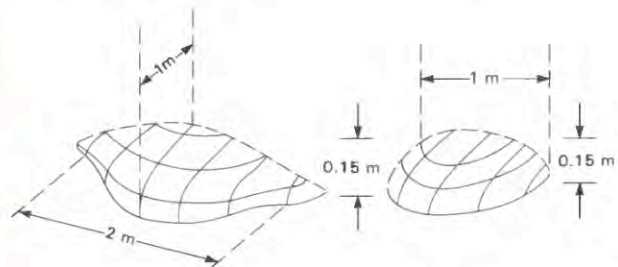


FIGURE 58.4.—Diagram illustrating two solidified overflow lobes at margin of channel at station 8. Lines are form lines.

center velocity, channel width, and estimated flow depth were of the order of $1.5 \times 10^6 \text{ m}^3/\text{h}$ (Lipman and Banks, chapter 57).

Two silvery lobes, interpreted to be recent overflows, were observed at the channel edge (fig. 58.4). They were estimated to be 0.15 m thick and 1–2 m wide; heat and the possible instability of the channel edge prevented direct measurements or sampling. These lobes are used later to estimate the yield strength of the lava, on the assumption that they represent solidified lava from the channel.

Postflow measurements indicate that the channel is 20 m wide and 6 m deep (Lipman and Banks, chapter 57, fig. 57.18, profile H). The estimated depth of flow was 4 m because the lava surface was 2 m below the channel lip during the eruption. The local slope derived from a 1:24,000-scale map is 5.6° .

STATIONS 4 AND 5, APRIL 3–7

Characteristics of the flow channels at these stations were diverse. The lava was confined within channels formed by high levees interspersed with sections reminiscent of station 8. In the high, leveed sections, topographic gradients were somewhat reduced. Upstream, lava flowed rapidly into the high, leveed part from channels with low overflow levees. Downstream, the levees, composed chiefly of rubble, increased in height and caused ponding of the lava, which spilled over the downstream side in a lava fall.

On April 3 near station 4 at an elevation of 1,920 m (6,300 ft), lava was flowing in a high, leveed channel with velocity as great as 1.2 m/s during surges and 0.8 m/s during ebbs. The levee was about 2.3 m high. Visible lava within the channel was composed of dark cinders and clinkers and incandescent clots set in a matrix of incandescent lava (fig. 58.5). Concentrations of the cinders and clinkers were larger than at station 8, and incandescent clots were not evident at station 8. Along the margin of the levee, the channel surface was crusted and stranded blocks were present (fig. 58.6A). During surges, rising lava would arch upward, and the marginal crusts and stranded blocks would sympathetically tilt upward and outward (fig. 58.6B). Surges were accompanied by small outward displacements of the levees and the avalanching of debris down the levee flanks. During peak surges the lava spilled over and onto the crust and stranded blocks (figs. 58.5A and 58.6C). During ebbs,



A



B

FIGURE 58.5.—Flow of 1984 Mauna Loa lava in high, rubbly, leveed channels. **A**, Station 4 on April 3. Lava from center during surge is overflowing material in channel at margin. Note dark, partly cooled lava. Channel is about 14 m wide. **B**, Station 6 on April 7. Typical flow in leveed channel during ebb. Note the structure and blocky appearance of incandescent clots. Channel is about 22 m wide.

the crust and blocks would become level as the lava subsided. Upstream, lava was flowing in a channel 14 m wide at 1.6 m/s. Here and elsewhere, swishing and shushing noises generated by the flowing lava were evident and more pronounced than those at station 8. The next day (April 4), the height of the rubbly levee had increased to 5 m. Upstream near the 1,935-m (6,350-ft) elevation, lava velocity was near 2 m/s; but the velocity varied somewhat because of surges and ebbs. On the morning of April 7 at station 5 at 1,950-m (6,400 ft), lava was flowing in the channel at 1.5 m/s; later in the day, lava overflowed the debris-choked leveed channel upstream and substantially reduced the input of the lava (fig. 58.6D, 58.7A). Lava from breakouts (fig. 58.7), or sudden releases of semi-ponded lavas, produced immense surges that overflowed the rubbly levees and formed a thin sheet over the levees and beyond to some distance from the levee crest; exceptionally large breakouts (fig. 58.7B) produced sustained flows such as flow 1B. Flow appeared to be laminar and nonturbulent during surges, ebbs,

and even breakouts. Distal lobes of a breakout sheet that probably occurred on April 6 were 0.3–0.75 m thick and 3–4 m wide (fig. 58.8). The thickness and width of these lobes are used later to estimate a yield strength for lava that flowed in the channel here.

Volume flow rates for the lava during April 2–5 were estimated to be in the range of 0.37×10^6 – 0.60×10^6 m³/h (Lipman and Banks, chapter 57).

STATION 1, APRIL 3

The flow at this station appeared in general to be a hummocky mass of slowly moving debris, rubble, and blocks confined within a rubbly, leveed channel 57 m wide and estimated to be 6 m deep (fig. 58.9). Mounds and blocklike incandescent units, partly to completely veneered by darker, cooler debris, rode along the top of the hummocky surface; at times, spallation of dark and incandescent debris would further expose their incandescent cores. Elsewhere, local exposures of incandescent lava beneath and intermingled with debris were common. The flow was unsteady, but not turbulent. Surges with velocity as great as 0.36 m/s were accompanied by increase in the height of the flow by a few meters; ebbs with velocity near 0.18 m/s were accompanied by decrease in the height of the flow by a few meters. Movement occurred by shearing between intact units along surfaces with traces that paralleled the channel edge (fig. 58.10). At intermediate velocities and thicknesses, the central part of the flow moved as a plug-like unit with little internal relative motion; the units immediately flanking the center moved at a slower velocity and, similarly, with little internal motion; and so on to the channel edges, where the velocity of the outermost units was very small to zero. As the flow surged and thickened, the velocity of the central unit increased and the relative velocities between the units decreased until, at peak velocity, almost the entire width between the levees had the same velocity. Estimates of the flowing width during two surges were 45 and 52 m. Surges were accompanied by crunching noises due to the grinding action between and within the intact units; the rubble levees were displaced outward and debris rolled down the levee flanks. As the flow ebbed and thinned, the velocity of the center unit decreased and that of the other units decreased sequentially outward from the center. Such ebbs were accompanied by a substantial decrease in noise; the levees ceased to move, and debris ceased to roll down their flanks. Further thinning would cause motion of the units to cease progressively from the channel edge toward the center. During one ebb, the entire flow briefly stopped. A visual estimate of the thickness at the center when that part ceased to move was 3 m.

Volume flow rates estimated during the eruption on April 3 were 0.15×10^6 to 0.45×10^6 m³/h (Lipman and Banks, chapter 57).

Post-eruption profiles of the channel suggest that it was 57 m wide and 8 m deep below the levee crest; a 2-m-thick layer of basalt occupied the channel floor (Lipman and Banks, chapter 57, fig. 57.18, profile M). The local slope derived from a 1:24,000-scale topographic map is 3.3°.

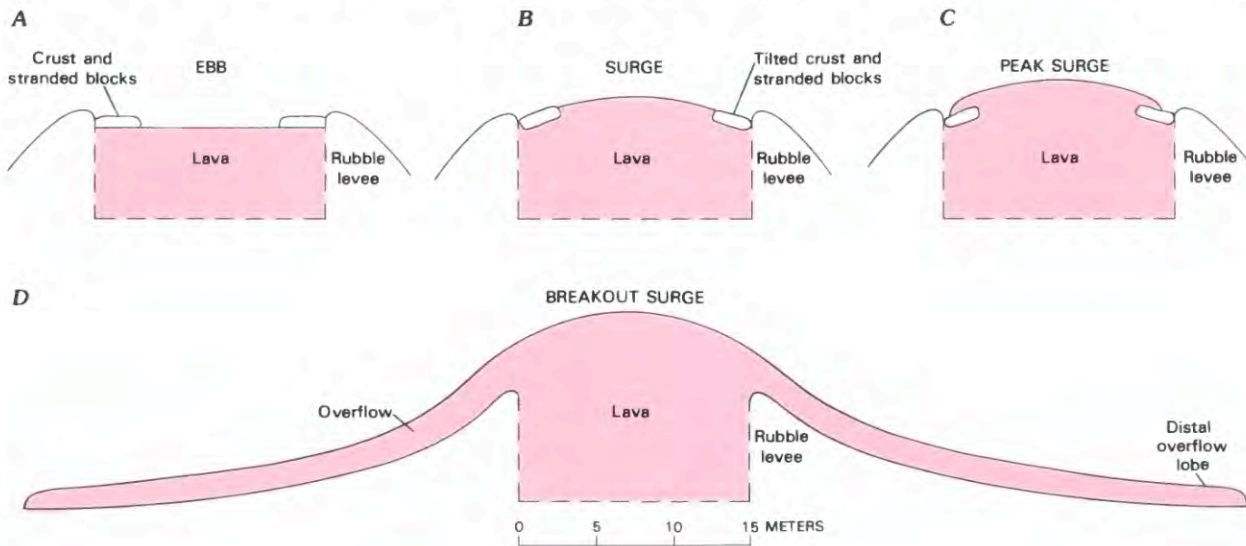


FIGURE 58.6.—Diagrammatic profiles of lava in channel with high, rubbly levees at station 4 on April 3 (A–C) and station 5 on April 7 (D). **A**, During ebb flow, marginal crusts, stranded blocks, and lava are nearly level. **B**, During surge flow, lava arches upward and marginal crust and stranded blocks tilt upward and outward. **C**, During peak surge, lava overflows tilted marginal crust and blocks. **D**, During breakout surge, lava spills over rubble levees and flows down levee flanks and onto surrounding surfaces, producing a deposit with lobate margins.

LOWER POWERLINE ROAD FLOW, APRIL 5

A wide unconfined flow 2–3 m thick, from a previous breakout, advanced eastward at a rate near 0.03 m/s on a slope of 3.6°. The flow was composed of an upper unit of blocks, clinkers, and cinders overlying incandescent molten lava (fig. 58.11). The

flow advanced in caterpillar-tractor style (Krauskopf, 1948): debris of the top layer moved faster than the underlying lava so that it avalanched down the advancing front and was overridden by the molten lower part (fig. 58.12A). The flow made crunching noises similar to those at station 1 and the avalanching debris made



FIGURE 58.7.—Breakout surges near stations 4 and 5. **A**, Breakout surge of April 7 from ponded lava upstream of station 5. Dark horizon to right is near crest of channel levee. Lava spills over levee near huge glob of incandescent lava that is moving toward the right. Overflows like this one produce layers with lobate margins on the flanks of the leveed channels. **B**, Breakout near station 4 on April 5. Note reddish-orange glowing lava overflowing levee and flowing down levee flank at left middle. Protrusions on center skyline are large (approx. 8-m) blocks carried along the leveed channel by lava flowing toward the left. Glowing lava in foreground and at right is part of breakout that produced flow 1B.

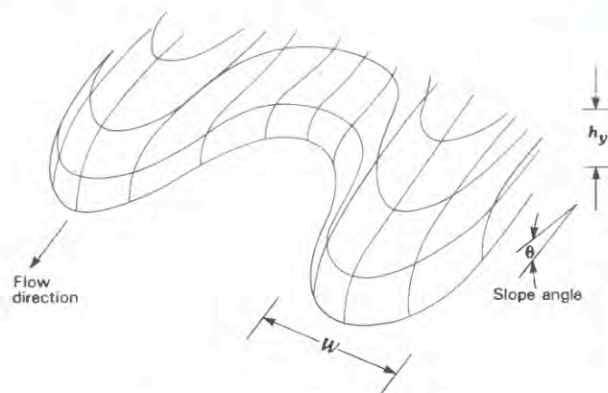


FIGURE 58.8.—Diagram of lobes at margin of overflow sheet from breakout surge on April 6 near station 5. Parameters indicated are lobe width (W), lobe thickness (h_y), and slope angle (θ).

clinking, thinking sounds. In most places the base of the molten lava was in contact with debris, but locally with preflow surfaces. Where exposed, the molten lava at the front of the flow was smoothly curved and showed subtle rounded protrusions here and there (fig. 58.12B). At the very base, it curved back upon itself, indicating that molten lava was overriding molten lava and that the velocity at the base of the flow was zero; debris in the process of being overridden was stationary. Large expanses of the upper surface moved downstream as intact units with little internal relative movement, although there was movement between the various intact units. In plan view the front was lobate, and each lobe tended to follow local rilles. The entire flow advanced down a broad, shallow valley.

FLOW 1A, APRIL 2–3

Although the toe of flow 1A could not be visited because of the dense vegetation there, it was estimated from the air to be 9 m thick and 762 m (2,500 ft) wide, and to be moving at 26 m/h on April 2 and 12 m/h on April 3. The local slope derived from a 1:24,000-scale topographic map is 3.65° . Crude estimates obtained by multiplying the thickness, width, and rate of advance indicate volume flow rates of $0.18 \times 10^6 \text{ m}^3/\text{h}$ on April 2 and $0.08 \times 10^6 \text{ m}^3/\text{h}$ on April 3. For an assumed density of $2,400 \text{ kg/m}^3$ (2.4 g/cm^3), the mass flow rates are $0.43 \times 10^9 \text{ kg/h}$ on April 2 and $0.20 \times 10^9 \text{ kg/h}$ on April 3.

MODELS AND EQUATIONS

MODELS

In the calculations below, the Mauna Loa lava flows are treated as Newtonian and Bingham fluids flowing in semi-elliptical channels and as wide, unconfined flows; flow is laminar. The implications of possible pseudoplastic flow are also considered.



FIGURE 58.9.—Surging flow at station 1 on April 3. Flow is composed chiefly of blocks, clinkers, and cinders and is moving from right to left. Spalling of debris from one block has exposed its reddish-orange molten core; some incandescent lava is also visible in ridge just below block. Immediate foreground is rubble levee; flow obscures levee on opposite side of channel. Large block at crest of flow is about 2 m across.

A Newtonian fluid is characterized by a viscosity (fig. 58.13). Here, the stresses are always proportional to the rate of shear. At high temperature, dense molten lava is a Newtonian fluid with a viscosity that is a function of composition and temperature (Shaw, 1969, 1972).

In contrast to a Newtonian fluid, a Bingham fluid is characterized by a yield strength in addition to a viscosity (fig. 58.13). The concept of a Bingham fluid was developed to account for the rheological behavior of paints flowing in circular pipes (Bingham, 1922) and later applied with success to the flow of slurries in pipes (Caldwell and Babbitt, 1941; Smith, 1960; Valentyik, 1972). Bingham (1922) suggested that his concept might apply to the flowage of some natural fluids such as lava. Subsequently, numerous authors have attempted to apply Bingham's fluid model to lava flows (Hulme, 1974; Moore and Schaber, 1975; Borgia and others, 1983; Cigolini and others, 1984), debris flows (Johnson, 1970; Fink and others, 1981), and landslips. Bingham-fluid concepts have been invoked by Kilburn (1981) to account for the irreversible transition of pahoehoe to aa (Macdonald, 1953) as described by Peterson and Tilling (1980). There is, however, a general lack of data on yield strengths and Bingham viscosities; such measurements are represented by the pioneering work of Shaw and others (1968) and subsequent works (Sparks and others, 1976; Cigolini and others, 1984).

A pseudoplastic fluid is different from both the Newtonian and Bingham fluids (fig. 58.13). Stresses on the pseudoplastic fluid produce rates of shear that vary according to a power law, and there is no single value of viscosity. Experimental data indicate that basalt at $1,120\text{--}1,125^\circ\text{C}$ behaves like a pseudoplastic fluid when stresses are less than about $16 \times 10^3 \text{ Pa}$ and shear rates are less than 5 s^{-1} (Shaw, 1969).

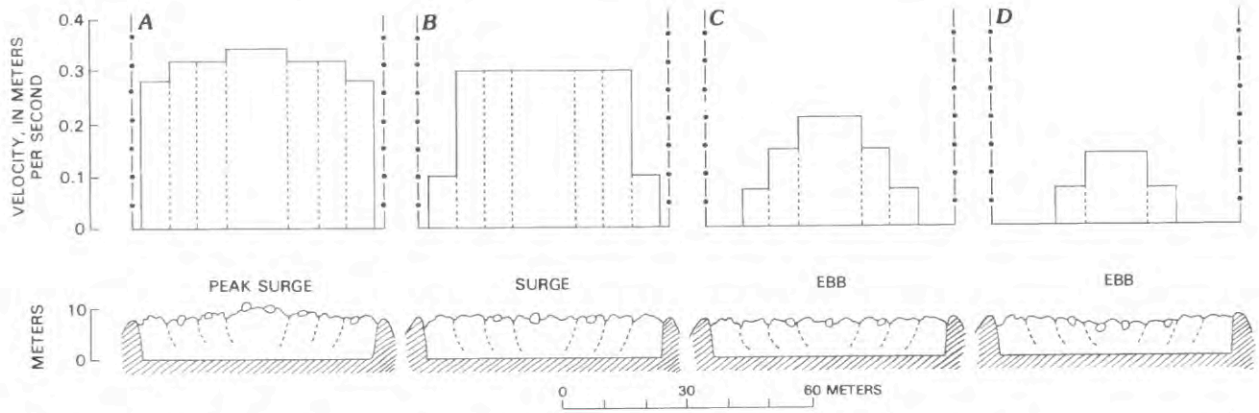


FIGURE 58.10.—Velocity profiles and diagrammatic cross sections of the unsteady flow of lava at station 1 on April 3. Dot-dash lines on velocity profiles represent crests of levees; dashed and solid lines outline discrete intact units of moving surface. Cross sections show upper surface of flow; dashed lines represent postulated unit boundaries (which may actually be vertical). **A**, During peak surge, surface of flow moves as discrete, intact units with velocities as great as 0.34 m/s; parts of center of flow are a few meters higher than levee crest. **B**, During surge, entire central 45 m of surface moves with a velocity near 0.3 m/s; velocities of units near edge are much less; surface of flow is about same elevation as levee crest but irregular. **C**, During ebb, a central unit moves as a plug with a velocity near 0.2 m/s; velocity decreases outward toward levee and that of units at edges is zero; elevation of surface of flow drops below elevation of levees. **D**, With further ebbing, central unit moves with a velocity near 0.15 m/s; next adjacent unit is slower; other units have stopped; surface of flow sags downward toward center.

APPARENT VISCOSITY

In an ideal Newtonian fluid, the viscosity is constant, and miniscule stresses produce miniscule rates of shear. In an ideal Bingham fluid, the viscosity is constant, but the rate of shear is zero when the stresses are less than the yield strength (fig. 58.13). Apparent viscosity, which is calculated in the same way as the Newtonian viscosity, is a strong function of the rate of shear for the



FIGURE 58.11.—Flow at Lower Powerline Road on April 5. Flow is about 3 m thick and advancing at a rate near 0.03 m/s. Upper surface is composed chiefly of debris; underlying reddish-orange layer of incandescent lava is locally exposed along front.

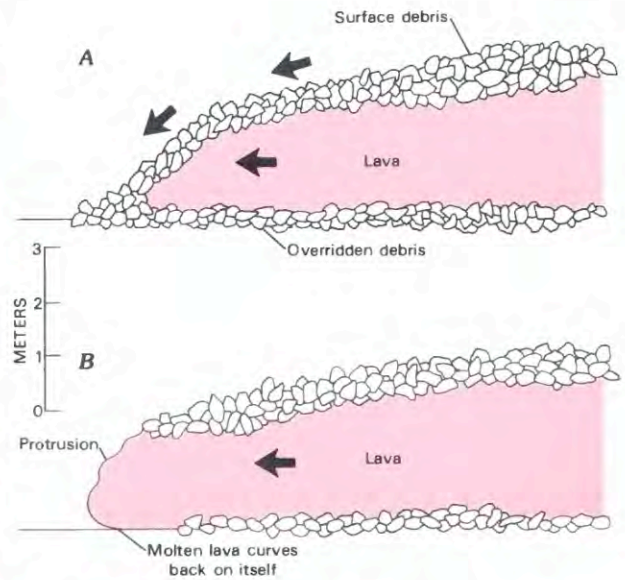


FIGURE 58.12.—Diagrammatic profiles of flow at Lower Powerline Road on April 5. **A**, The flow is typical aa, with an upper surface of debris overlying molten, incandescent lava. Upper surface moves as a unit with greater speed than underlying layer so that debris avalanches and falls down front and is then overridden by flow. **B**, Surface of molten lava. Where surface of molten lava is exposed at the front, it is smoothly curved, with some rounded protrusions, and curves back upon itself at the base.

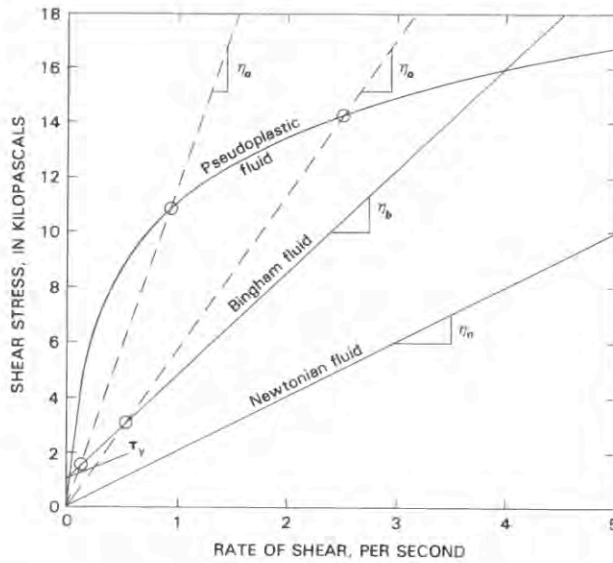


FIGURE 58.13.—Relation between shear stress and rate of shear for Newtonian, Bingham, and pseudoplastic fluids. Newtonian fluid is represented by straight line passing through origin; slope of line (η_n) is the viscosity. Bingham fluid has a yield strength (τ_y) and a viscosity; shear stress on Bingham fluid must exceed the yield strength (τ_y) to produce a rate of shear greater than zero; slope of line (η_b) is the Bingham viscosity. Pseudoplastic fluid is represented by curved line; rate of shear is approximately a function of shear stress raised to some power. Apparent viscosity (η_a) assumes a Newtonian fluid and varies with the rate of shear for Bingham and pseudoplastic fluids. As depicted, viscosity of Newtonian fluid is 2×10^3 Pa·s. Viscosity and yield strength of Bingham fluid are 3.8×10^3 Pa·s and 10^3 Pa, respectively. Pseudoplastic fluid is similar to basalt at $1,125^\circ\text{C}$ (Shaw, 1969).

Bingham fluid. It varies from large values at small rates of shear to values that approach the Bingham viscosity at very large rates of shear. Similarly, apparent viscosity calculated for a pseudoplastic fluid varies from large values at small rates of shear to smaller values at larger rates of shear. The term “apparent viscosity” is applied to calculations for any fluid when the fluid is assumed to be Newtonian (see, for example, Shaw, 1969).

PLUGS AND SLABS

As a consequence of the yield strength, the central and upper parts of Bingham fluids flowing in the laminar regime move as plugs in channels and as slabs in wide, unconfined flows (Johnson, 1970). Dimensions of the plugs and slabs depend on the stresses acting on the fluid, the yield strength, and the shape and size of the channel or wide flow. The velocity distribution from the margins of a flow in a semi-elliptical channel to the central plug, or from the base of the wide flow, is the same as the normal velocity distribution for laminar flow of a Newtonian fluid; velocity increases from zero at the margin or base of the flow to the velocity of the plug or slab at its edge. For a Newtonian fluid, the dimensions of the plug or slab are zero.

EQUATIONS

The yield strength of a Bingham fluid may be estimated from the dimensions of the flow at rest and the plug or slab dimensions when the fluid is flowing. Viscosity for both Newtonian and Bingham fluids may be estimated from the observed velocity. Additional parameters required for these estimates include the acceleration of gravity, fluid density, slope angle or topographic gradient, and channel or flow dimensions. Equations used for these estimates are described below.

YIELD STRENGTH

Yield strength (τ_y) can be estimated from the rest thickness (h_y) of a wide, unconfined Bingham fluid that has stopped. The stress acting on this flow (τ), which is driven by gravity, is given by:

$$\tau = \rho g h \sin \theta \quad (1)$$

where ρ is the density of the flow, g is the acceleration of gravity, h is the distance below the surface of the flow, and $\sin \theta$ is the topographic gradient (θ is the slope angle measured at a characteristic flow surface). The stress at the base of the flow (τ_b) is obtained when h is equal to the thickness of the flow during flow (H). The stress at the base of the slab, which is equal to the yield strength (τ_y), is obtained when h is equal to the thickness of the slab (h_y). A wide, unconfined flow comes to rest when the shear stress (τ) is less than the yield strength at all depths. This may occur because the flow thins or the yield strength increases. Because τ is a maximum at the base of the flow,

$$\tau_y = \rho g h_y \sin \theta \quad (2)$$

where τ_y is the yield strength of the flow and h_y is the slab thickness or rest thickness of the flow.

Yield strength can be estimated from flow lobes at rest because the viscosity is no longer important and the flow may therefore be treated as a plastic. According to Orowan (1949), the yield strength of a plastic body can be obtained from the relation:

$$\tau_y = \rho g h_y^2 / W \quad (3)$$

where W is the width of the lobe.

Yield strength may also be estimated from the dimensions of the plug of a Bingham fluid flowing in a channel. For a flow driven by gravity in a semi-elliptical channel, Johnson (1970) obtains the relations:

$$\tau_y = \rho g a_y \sin \theta / [(A/B)^2 + 1] \quad (4)$$

and

$$\tau_y = \rho g b_y \sin \theta / [(B/A)^2 + 1] \quad (5)$$

where a_y is the half-width of the plug, b_y is the thickness of the plug, A is the half-width of the channel or flow, and B is the depth of flow in the channel center.

VISCOSITY

Viscosity of the Mauna Loa lava can be calculated because the velocity of the flowing lava at the centers of channels (V_o) and the channel width were measured and good estimates of flow depth were obtained during the eruption (Lipman and Banks, chapter 57). Viscosity (η) is calculated using an equation for laminar flow in semi-elliptical channels (after Johnson, 1970):

$$\eta = (\rho g \sin \theta / V_o) \{ B^2/2[(B/A)^2 + 1] + [(B/A)^2 + 1][\tau_y/\rho g \sin \theta]^2/2 - \tau_y B/\rho g \sin \theta \} \quad (6)$$

where B is the depth of flow in the channel center and A is the half-width of channel or flow.

The application of equation 6 needs some discussion; profiles of channels obtained after the eruption indicate that most of them were more or less rectangular (Lipman and Banks, chapter 57, fig. 57.18, table 57.2), whereas equation 6 assumes that the channels are semi-ellipses; the semi-ellipses are inscribed in the rectangular channels and defined by the depth of flow and the half-width of the channel or flow. Additionally, the lava is treated as both a Newtonian and a Bingham fluid in later calculations. When B/A is zero, equation 6 yields the correct expression for laminar flow of a Bingham fluid in an infinitely wide channel or as a wide, unconfined flow. When both B/A and the yield strength (τ_y) are equal to zero, equation 6 yields the correct expression for laminar flow of a Newtonian fluid in an infinitely wide channel or as a wide, unconfined flow. Similarly, when B/A is one, equation 6 yields the correct expression for laminar flow of a Bingham fluid in a semicircular channel. When B/A is one and the yield strength is zero (τ_y), equation 6 yields the correct expression for laminar flow of a Newtonian fluid in a semicircular channel. Intuitively, it seems probable that apparent viscosity calculated for rectangular channels would be reasonably close to that calculated with equation 6. Viscosity of a Newtonian fluid assuming an infinitely wide channel with a depth of B is twice as large as that assuming a semicircular channel with a radius of B because B/A ranges from zero to one; these two conditions should bracket the rectangular channels in most cases (see, for example, Lipman and Banks, chapter 57). For a Bingham fluid, the yield strength results in dead zones (no motion) at the bottom corners of rectangular channels (Johnson, 1970); semi-elliptical channels may therefore be reasonable approximations. Finally, Johnson (1970, p. 505) states that equation 6 may be applied to flows in rectangular and triangular channels with sufficient accuracy for most purposes. Thus, the preliminary viscosities calculated below are believed to be reasonable estimates; but subsequent studies should employ theories for flow in rectangular channels.

AVERAGE VELOCITY

Average velocity is lower than plug or slab velocity to a varied degree that depends on the yield strength, viscosity, stress, and channel or flow geometry. For flow of a uniformly thick Bingham fluid in very wide channels or as wide flows, the average velocity is

given by

$$\bar{V} = (H^2 \rho g \sin \theta / 3\eta) [1 - (3/2)(\tau_y/\tau_b) + (1/2)(\tau_y/\tau_b)^3]. \quad (7)$$

For a Newtonian fluid ($\tau_y = 0$), equations 6 and 7 show that the average velocity is two-thirds the velocity at the surface. For flow of a Bingham fluid in semicircular channels, the average velocity is given by

$$\bar{V} = (R^2 \rho g \sin \theta / 8\eta) [1 - (4/3)(\tau_y/\tau_b) + (1/3)(\tau_y/\tau_b)^4]. \quad (8)$$

For a Newtonian fluid ($\tau_y = 0$), equations 6 and 8 show that the average velocity is one-half the velocity at the channel center.

An explicit equation for average velocity in an elliptical channel is not available to the author at this time. For this reason, estimates were made of the lower and upper bounds for the average velocity. The lower and upper bound estimates use the fact that the average velocity of flow between the plug and margin of a circular channel is between one-half and two-thirds of the velocity of the plug; the average velocity of flow between the slab and base of a wide, unconfined flow is two-thirds the velocity of the slab.

MASS AND VOLUME FLOW RATES

Volume flow rate is the product of the average velocity and the flow cross-sectional area. Mass flow rate is the product of flow density and volume flow rate. Here, the assumption of semi-elliptical channels may affect the results somewhat because the area of the semi-ellipse inscribed in a rectangular channel is 0.79 times the area of the rectangle. Thus, the volume and mass flow rates for a Newtonian fluid flowing through a semi-elliptical area is 0.39–0.52 times the volume and mass flow rates calculated by multiplying the center velocity and a rectangular area. These factors are less for a Bingham fluid in a variable way that depends on the size of the plug.

CRITERIA FOR LAMINAR FLOW

The use of the equations above assume laminar flow; the modified Reynolds number (R_m) must therefore be sufficiently low. For wide flows (Moore and Schaber, 1975),

$$R_m = 2[(\eta/\rho \bar{V}H) + (\tau_y/2\rho \bar{V}^2)] \quad (9)$$

where H is the thickness of the flow; and for flows in semicircular channels (Smith, 1960),

$$R_m = 2[(\eta/\rho \bar{V}R) + (\tau_y/4\rho \bar{V}^2)] \quad (10)$$

where R is the radius of the channel. Similar expressions for elliptical channels are not available at this time, but the above equations should give reasonable estimates of whether a flow is either laminar or turbulent.

RESULTS

DATA USED

In the calculations of apparent viscosity, I have used in all cases the flow velocities, channel widths, and flow depths reported by

TABLE 58.1.—Densities used to calculate apparent viscosity, Bingham viscosity, yield strength, volume flow rate, and mass flow rate

[Slope angles listed were used in calculations of apparent viscosity. See Lipman and Banks (chapter 57) for dates, times, sample numbers, sample densities, and sample descriptions]

Station	Elevation		Density (kg/m ³)	Slope angle (degrees)	Date (mo/d/yr)	Time (H.s.t.)	Sample	Density (kg/m ³)	Sample Description
	(m)	(ft)							
1	1620	5300	2400	3.3	3/25/84	1540	NER-1F	2230	Core of aa flow.
2	1710	5600	2200	4.0	3/29/84	1300	-----	2600	Core of aa flow.
3	1800	5900	2000	2.5					
3	1800	5900	1700	2.5					
4	1920	6300	1700	2.5					
4	1935	6350	1700	3.5	4/06/84	1430	NER-12/48	1720	Overflow from main channel.
4	1920	6300	1700	3.0					
5	1950	6400	1700	2.5					
6	2100	6900	1700	4.0					
7	2290	7500	1300	4.5	4/08/84	1306	NER-12/57	1250	Overflow from main channel.
8	2500	8200	1000	6.0	4/06/84	1220	NER-12/47	1150	From main channel.
8	2500	8200	1000	5.0	4/08/84	1026	NER-12/53	990	From main channel.
11	2850	9350	530	6.5	4/08/84	1145	NER-12/54	530	Overflow from main channel.
12	2870	9400	530	3.0					
12	2870	9400	530	4.5					

Lipman and Banks (chapter 57). Values for one case (station 11, vent, April 8, 1600 H.s.t.) appear to yield a spurious result, which is graphically reported but omitted from the discussion below. Slope angles also come from the same source, with the exceptions of station 1, which was 3.3° instead of 3°, and station 6 (April 7), for which the author obtained 4°. No slope angles are reported for stations 9 and 10. Flow densities employed are listed in table 58.1 and were selected by the author from values reported by Lipman and Banks (chapter 57). The acceleration of gravity is taken as 9.8 m/s². According to unpublished Hawaiian Volcano Observatory staff reports, flow 1A advanced at a rate of 7.2×10^{-3} m/s on April 2 and 3.4×10^{-3} m/s on April 3; given a thickness of 9 m, equation 7 yields apparent viscosities near 5.6×10^6 Pa·s (April 2) and 12×10^6 Pa·s (April 3). Calculated apparent viscosities are reported graphically (fig. 58.14) and described below.

APPARENT VISCOSITY

There are two general trends in the magnitude of the apparent viscosity (fig. 58.14). First, apparent viscosity increases dramatically along the length of the flow on a given day. On April 2, for example, apparent viscosities were: (1) 1.4×10^2 Pa·s at the vent (station 11); (2) 1.0×10^3 – 1.3×10^3 Pa·s 3 km from the vent at station 8; (3) 3.0×10^3 – 9.5×10^3 Pa·s 9 km from the vent at station 4; (4) 0.9×10^5 – 1.6×10^5 Pa·s 15 km from the vent at station 1; and (5) 5.6×10^6 Pa·s 26 km from the vent at the toe of flow 1A. Second, apparent viscosity at some stations increases with time. In the vent area, for example, apparent viscosities were

1.4×10^2 – 1.6×10^2 Pa·s (station 11) and more or less constant from April 2 through April 6, but they increased to 2.7×10^2 – 4.5×10^2 Pa·s (stations 11 and 12) on April 8 and 9 (excluding one value for April 8 that is assumed to be spurious); they climbed to 0.9×10^3 and 1.4×10^3 Pa·s (station 12) on April 12 and 13, respectively. At the 1,620-m (5,300-ft) level (station 1) apparent viscosity increased from about 1.6×10^4 Pa·s on March 31 to 0.5×10^5 – 1.5×10^5 Pa·s on April 2, 3, and 4. At some stations, such as station 4, the behavior of the apparent viscosity is mystifying. At 1,920 m (6,300 ft), it was 3×10^3 – 6×10^3 Pa·s on March 29 and by April 2 had increased to 9.5×10^3 Pa·s. Upstream, at 1,935 m (6,350 ft), the apparent viscosity on April 2 was 3×10^3 Pa·s, fully one-third of that downstream. The magnitudes of the calculated apparent viscosity will be compared with experimental data on basalt, and factors that may account for them will be discussed later.

BINGHAM LAVA

Three idealized stations and flow conditions are used below to examine the effects of a Bingham fluid on the lava rheology and consider volume and mass flow rates on a given day. These idealized conditions correspond to conditions on April 3 at (1) station 8, (2) station 4, and (3) station 1. The idealized channel and flow conditions (tables 58.2, 58.3, and 58.5) are slightly changed from those used in the calculations of apparent viscosities and listed in Lipman and Banks (chapter 57); the latter are given in tables 58.2, 58.3, and 58.5 as observations and estimates. Some of the calculations test a proposed equation relating viscosity and yield strength

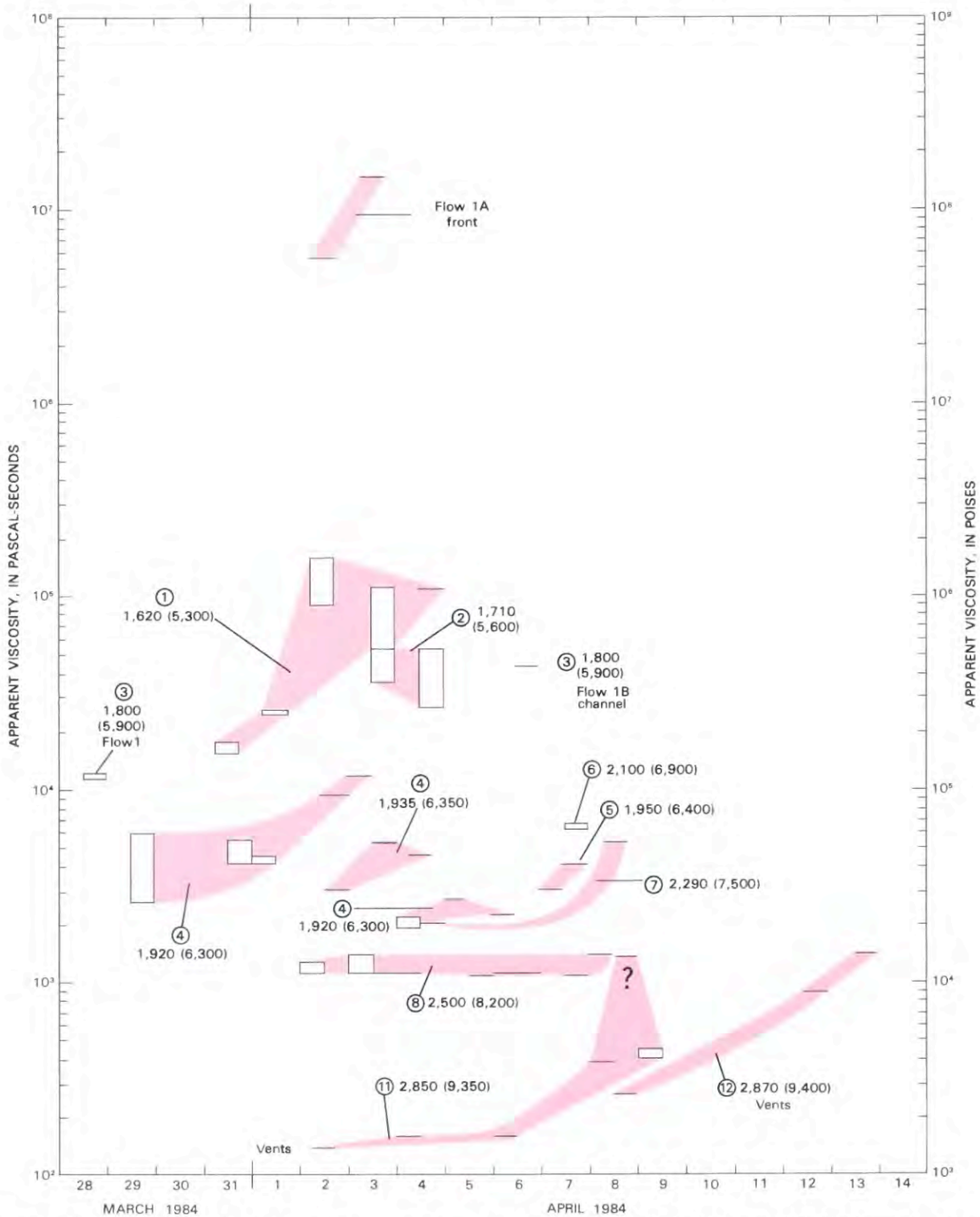


FIGURE 58.14. — Apparent viscosity of Mauna Loa lava at various stations from March 28 through April 13. Graphs of data connected by shaded areas indicate the same station or locality on different days. Station numbers circled from Lipman and Banks (chapter 57, table 57.3). Figures give elevation in meters (elevation in feet in parentheses). One determination for April 8 (queried) is probably spurious. Note that (1) apparent viscosity increases greatly from higher to lower elevations or with distance from vent on any given day from March 31 through April 8 and (2) apparent viscosity increases with time at the vents and at many of the stations downstream of the vents.

TABLE 58.2.—Observations and calculations for idealized station 8 on April 3

[Station is at 1852 vent, 2,500 m (8,200 ft) elevation]

Speed at center, \underline{V} (m/s)	Flow depth, \underline{B} (m)	Channel width, $\underline{2A}$ (m)	Volume flow rate, \underline{Q} ($10^6 \text{ m}^3/\text{h}$)	Mass flow rate, \underline{M} (10^9 kg/h)	Yield strength, $\underline{\tau}_y$ (Pa)	Viscosity, $\underline{\eta}$ Pa·s	Assumed density, $\underline{\rho}$ (kg/m^3)	Slope angle, $\underline{\theta}$ (degrees)
Observations and estimates								
5.3	4	20	1.5	1.5	—	—	1000	5.0
Calculations								
5.3	4	20	0.6–0.8	0.6–0.8	¹ 0	1244	1000	5.6
5.3	4	20	0.6–0.8	0.6–0.8	² 66	1195	1000	5.6
5.3	4	20	0.6–0.8	0.6–0.8	³ 221	1083	1000	5.6
5.3	4	20	0.6–0.8	0.6–0.8	⁴ 150	1134	1000	5.6

¹yield strength set to zero in equation 6; viscosity is apparent viscosity.²yield strength calculated from half-width of plug (0.5 m) (eq. 4); viscosity from equation 6.³yield strength calculated from rest widths and heights of flow lobes at channel edge (eq. 3); viscosity from equation 6.⁴yield strength adjusted until velocity of plug was satisfied with a viscosity from equation of Moore (1982), calculated plug width is 2.3 m.

TABLE 58.3.—Observations and calculations for sections at idealized station 4 on April 3

[Station is at 1,920–1,935 m (6,300–6,350 ft) elevation]

Speed at center, \underline{V} (m/s)	Flow depth, \underline{B} (m)	Channel width, $\underline{2A}$ (m)	Volume flow rate, \underline{Q} ($10^6 \text{ m}^3/\text{h}$)	Mass flow rate, \underline{M} (10^9 kg/h)	Yield strength, $\underline{\tau}_y$ (Pa)	Viscosity, $\underline{\eta}$ Pa·s	Assumed density, $\underline{\rho}$ (kg/m^3)	Slope angle, $\underline{\theta}$ (degrees)
Observations and estimates								
0.94	7	18.3	0.43	0.74	—	—	1700	2.5
1.6	5	14	0.40	0.69	—	—	1700	3.5
Calculations, lower section								
1.0	6	18	0.15–0.20	0.26–0.34	¹ 0	7245	1700	2.0
1.0	6	18	0.17–0.22	0.29–0.37	² 684	3723	1700	2.0
1.0	6	18	0.21–0.24	0.35–0.41	³ 1185	1880	1700	2.0
1.0	6	18	0.18–0.22	0.31–0.38	³ 891	2885	1700	2.0
Calculations, upper section								
1.6	5	14	0.16–0.21	0.27–0.36	¹ 0	5637	1700	3.75
1.6	5	14	0.17–0.22	0.28–0.37	² 684	3702	1700	3.75
1.6	5	14	0.18–0.23	0.31–0.39	² 1185	2542	1700	3.75
1.6	5	14	0.17–0.22	0.30–0.38	³ 970	3014	1700	3.75

¹yield strength set to zero in equation 6; viscosity is apparent viscosity.²yield strength calculated from dimensions of flow lobes (eqs. 2, 3); viscosity from equation 6.³yield strength adjusted until velocity of plug was satisfied with viscosity from equation of Moore (1982); dimensions required for plug are 2.2 m by 10.0 m and 2.6 by 5.2 m.

TABLE 58.4.—*Dimensions, slopes, and yield strength of overflow lobes at station 5*
 [Overflows probably occurred late on April 6]

Lobe	Width, W (m)	Thickness, t		Slope angle, θ (degrees)	Yield Strength, τ_y	
		Range (m)	Average (m)		from equation 2 (Pa)	from equation 3 (Pa)
1	3	0.45–0.60	0.53	5.5	846	1531
2	4	0.60–0.75	0.68	1–2.5 (1.75)	346	1898
3	3	0.45	0.45	6	784	1125
4	4	0.60–0.75	0.68	4	790	1926
5	4	0.30–0.45	0.38	6	662	601
6	4.5	0.30–0.45	0.38	3	331	535
7	3	0.35	0.35	10	1013	680
8	—	0.60	0.60	4	698	—
Average					684	1185

(Moore, 1982); others deal with a wide, unconfined flow and a channel flow at the vent, although the channel flow is not treated as Bingham fluid. The results are plotted in figure 58.15, from which it can be seen that Bingham viscosity and yield strength exhibit striking increases along the length of the flow; yield strength increases about 10–34 times from station 8 to station 1, and Bingham viscosity increases about 70–80 times.

STATION 8

The parameters used for this station (table 58.2) are identical to those used for the calculation of apparent viscosity except for a slope of 5.6° instead of 5° or 6° .

Yield strength for the lava at this location is on the order of 10^2 Pa (table 58.2). Two methods were used in preparing the estimates. In the first method, the half-width of the plug observed by the author (0.5 m), inserted in equation 4, gives a result of 66 Pa. In the second, the height (0.15 m) and width (1.0 m) of the lobes at the channel edge (fig. 58.7), inserted in equation 3 give a result of 221 Pa; if the lobe width is taken as 2.0 m instead of 1.0 m, the yield strength becomes 110 Pa. The larger yield strength requires a plug 3.4 m across instead of the observed 1.0 m.

Bingham viscosity does not differ significantly from the apparent viscosity of 1.2×10^3 Pa·s. For the largest yield strength the viscosity is about 1.1×10^3 Pa·s. Finally, the observed 5.3 m/s velocity of the plug can be obtained when the yield strength and viscosity, derived from the proposed equation of Moore (1982), are 150 Pa and 1.1×10^3 Pa·s, respectively; the calculated plug width is 2.3 m.

It should be noted that the calculated modified Reynolds numbers, which are in all cases 29 or less, are in agreement with the observed laminar character of the flow. The results are plotted in figure 58.15.

STATION 4

The actual channel and flow conditions at this station were rather complicated, some sections having high, rubbly levees and others low to nonexistent overflow levees. For the idealization of this station, three noteworthy changes in particular were made from those used to calculate apparent viscosity: (1) the slope for the lower section with high, rubbly levees was changed from 2.5° to 2.0° ; (2) the flow depth of the lower section was changed from 7 m to 6 m; and (3) the slope of the upper section with low to nonexistent levees was changed from 3.5° to 3.75° (table 58.3). These changes were made in order to satisfy the requirement of conservation of mass and still have the same Bingham fluid properties in two adjacent sections.

Yield strength for this station is probably near 10^3 Pa. Average values for yield strength calculated with equations 2 and 3 and dimensions of lobes at the margin of an overflow sheet are 684 and 1,185 Pa, respectively (table 58.4). There is some uncertainty in correlation because the overflow producing the sheet probably occurred on April 6, not April 3.

Apparent viscosities required to account for the 1.0 m/s and 1.6 m/s velocities in the idealized lower and upper sections are 7.6×10^3 Pa·s and 5.6×10^3 Pa·s, respectively; the mass flow

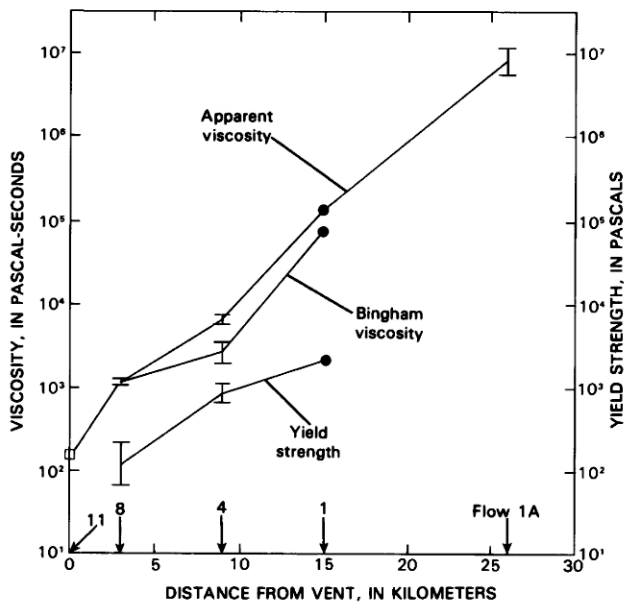


FIGURE 58.15.—Apparent viscosity, Bingham viscosity, and yield strength as a function of distance from vents on April 3. Numbers and arrows on abscissa indicate stations and their distances from vents. Note that Bingham viscosity shows increase in magnitude comparable to that of apparent viscosity. Value for station 11 (open square) is from text; values for station 1 (dots) are from table 58.5; vertical lines for stations 8 and 4 show range of values from tables 58.2 and 58.3; vertical line for flow 1A shows range of values from text.

rates are substantially the same (table 58.3). A Bingham fluid with a yield strength near 680 Pa and a viscosity near 3.7×10^3 Pa·s would conserve mass and provide the same rheology for the lava at the two adjacent sections. Calculations using the larger yield strength of 1,185 Pa do not yield the same viscosity, but the two values are close. Finally, values of yield strength and viscosity from Moore's (1982) equation that satisfy the velocity in equation 6 are reasonably close both to one another and to the values derived from equations 2 and 3.

It should be noted that modified Reynolds numbers, which are less than 11 in all cases, are in agreement with the observed laminar character of the flow. Results are plotted in figure 58.15.

STATION 1

A simple Bingham fluid cannot account for the flow at this station because it does not explain the occurrence of a number of discrete, intact flow units between the center plug and the channel margin, the velocity gradient of the flow units across the channel increases with ebbing and with lower center velocity, and the Bingham model has nothing to say about nonsteady flow. In one set of calculations that employ a constant channel width, the width of the plug becomes greater than the width of the channel with thinning of the flow. Such a condition would seem to require faulting or shearing of the plug, which could result in a number of discrete, intact flow units and variable yield conditions. In any event, however, the

Bingham model will be applied with the intention of illustrating the problem.

Channel dimensions and flow velocities employed below are different from those used for the calculation of apparent viscosity (table 58.5). The channel width and depth are taken as 57 m and 8 m, respectively, on the basis of the profile measured after the eruption. For the nominal conditions, a velocity of 0.3 m/s is paired with a flow depth of 8 m and a plug width of 45 m; these values are consistent with the author's impressions of the flow on April 3. The slope is taken as 3.3° . Subsequent calculations predict the velocity at the center of flow with varying flow depths using (A) a model with a fixed channel width (57 m) but varying flow depth, and (B) a model that assumes effective channel width varies directly with flow depth.

A yield strength of 2,225 Pa is used in the calculations (table 58.5). This value was obtained using equation 4 and the nominal conditions mentioned above; it is reasonably close to the 2,700 Pa obtained using a rest thickness of 2 m estimated from the lava on the channel floor in the postflow profile.

An apparent viscosity of 1.34×10^5 Pa·s is obtained for the nominal conditions of flow mentioned above (table 58.5); this is only 21 percent higher than the largest apparent viscosity obtained previously for April 3 (fig. 58.14). Incorporation of a yield strength of 2,225 Pa in equation 6 gives a Bingham viscosity of near 81×10^3 Pa·s (fig. 58.15). This viscosity is 17 times larger than the one predicted by Moore's (1982) equation. Modified Reynolds numbers for all flow calculations, which are discussed below, are less than 1 and consistent with laminar flow.

Calculations for model A (table 58.5) predict some of the salient aspects of the surging and ebbing flow and plug widths that become larger than the channel width with ebbing flow. At the nominal flow condition, the central 45 m of the flow moves as a plug with a velocity of 0.3 m/s. During a surge, the flow thickens to 9 m and the central 36 m of the flow moves as a plug with a velocity of 0.39 m/s. When the flow ebbs, the flow thins to 7 m and the central part of the flow moves as a plug with a velocity of 0.22 m/s. Here, the plug is about the same width as the channel so that some sort of interference of flow and disruption of the plug might be expected. With further thinning to 6 m, the predicted speed of the flow is 0.15 m/s, and the plug will no longer fit in the channel.

In model B, reasonable plug velocities are obtained by varying the yield strength during surging and redefining the channel dimensions during ebbs. For example, if the yield strength increases to 3,200 Pa because of increased friction by loading during a 9.3-m-thick surge, the velocity of the 49-m-wide plug is 0.34 m/s. If the channel is redefined to be 7 m deep and 42 m wide and the yield strength returns to 2,225 Pa, the velocity of the 33-m plug in the fluid-filled channel is 0.2 m/s. Narrower, shallower filled channels have smaller plug velocities, and the plugs do not reach the channel margins.

WIDE, UNCONFINED FLOWS

There is no information from which to estimate the yield strength and Bingham viscosity for the Lower Powerline Road flow

TABLE 58.5.— Observations and calculations using two models for idealized station 1 on April 3

[Station is in lower channel of flow 1A at 1,620 m (5,200 ft) elevation. For explanation of models see text]

Speed at center, V (m/s)	Flow depth, B (m)	Channel width, $2A$ (m)	Volume flow rate, Q ($10^6 \text{ m}^3/\text{h}$)	Mass flow rate, M (10^3 kg/h)	Yield strength, τ_y (Pa)	Viscosity, η Pa·s	Assumed density, ρ (kg/m^3)	Slope angle, θ (degrees)	Dimensions of plug, $b, 2a$ (m) (m)
Observations and estimates									
0.38	6	52	0.43	1.0	—	—	2400	3.0	—
0.3	6	52	0.34	0.82	—	—	2400	3.0	—
0.2	6	52	0.23	0.54	—	—	2400	3.0	—
Calculation of apparent viscosity									
0.3	8	57	0.19–0.26	0.46–0.62	¹ 0	133,800	2400	3.3	0.0, 0.0
Calculations using model A									
0.3	8	57	0.23–0.28	0.54–0.67	² 2225	81,110	2400	3.3	1.8, 45.0
0.39	9	57	0.32–0.40	0.77–0.97	2225	81,110	2400	3.3	1.8, 36.2
0.22	7	57	0.15–0.18	0.34–0.44	2225	81,110	2400	3.3	1.7, 57.8
0.15	6	57	0.09–0.11	0.23–0.28	2225	81,110	2400	3.3	1.7, 77.4
Calculations using model B									
0.34	9.3	57	0.31–0.38	0.75–0.91	³ 3200	81,110	2400	3.3	2.6, 49.1
0.3	8	57	0.23–0.28	0.55–0.67	² 2225	81,110	2400	3.3	1.8, 45.0
0.2	7	42	0.10–0.12	0.24–0.30	2225	81,110	2400	3.3	1.8, 32.9
0.13	6	35	0.05–0.06	0.12–0.14	2225	81,110	2400	3.3	1.8, 31.2
0.001	4	10	—	0.02	2225	81,110	2400	3.3	2.7, 8.4

¹Yield strength set to zero in equation 6; viscosity is apparent viscosity.²Yield strength calculated from half-width of plug (taken as 45 m) (eq. 4); viscosity from equation 6.³Yield strength assumed to increase with load during surge; viscosity same as in (2) above.

on April 5. If the flow, 3 m thick, had the same properties as those at station 1 ($\tau_y = 2,225 \text{ Pa}$, $\eta = 81 \times 10^3 \text{ Pa}\cdot\text{s}$), it would advance at a rate near 0.02 m/s and its rest thickness would be 1.5 m.

STATION 11

In order to consider volume and mass flow rates along the length of the flow on April 3, average values for April 2 and 4 must be used. On April 2, the lava was flowing in a channel 21.5 m wide with a flow depth of 3 m at 17.8 m/s; on April 4, the lava was flowing in a channel 21 m wide with a flow depth of 3 m at 15 m/s (Lipman and Banks, chapter 57). Volume flow rates from the average of these conditions are $3.8 \times 10^6 \text{ m}^3/\text{h}$ for a rectangular flow at uniform velocity and 1.5×10^6 – $2.0 \times 10^6 \text{ m}^3/\text{h}$ for laminar flow in a semi-elliptical channel. Mass flow rates are $2.0 \times 10^9 \text{ kg/h}$ for a rectangular flow and 0.8×10^9 – $1.1 \times 10^9 \text{ kg/h}$ for flow in a semi-elliptical channel. Apparent viscosities on the two days were near $0.15 \times 10^3 \text{ Pa}\cdot\text{s}$, and modified Reynolds numbers were less than 300 and indicate laminar flow.

VOLUME AND MASS FLOW RATES

This section presents calculated volume and mass flow rates for April 3 along the length of the flow (fig. 58.16) from the vent to the toe. In these calculations, I have used the parameters for the idealized stations (tables 58.2, 58.3, and 58.5), the estimates for the vent given in the previous section, and approximate calculations for the toe. Because of the surging, ebbing flow at station 1, average volume and mass flow rates are difficult to estimate; for purposes of illustration, volume and mass flow rates are taken as those corresponding to velocities of 0.2 and 0.22 m/s in table 58.5. A small overflow upstream of station 1 on the morning of April 3 does not apparently affect the results because the magnitude of changes is much the same as on April 2.

Volume flow rates appear to decrease by about one order of magnitude from the vent to station 1, beyond which estimates are so uncertain that a decrease may or may not be present (fig. 58.16A). The volume flow rates calculated for a rectangular flow with uniform velocity are $3.8 \times 10^6 \text{ m}^3/\text{h}$ at the vent, $1.5 \times 10^6 \text{ m}^3/\text{h}$ at station 8,

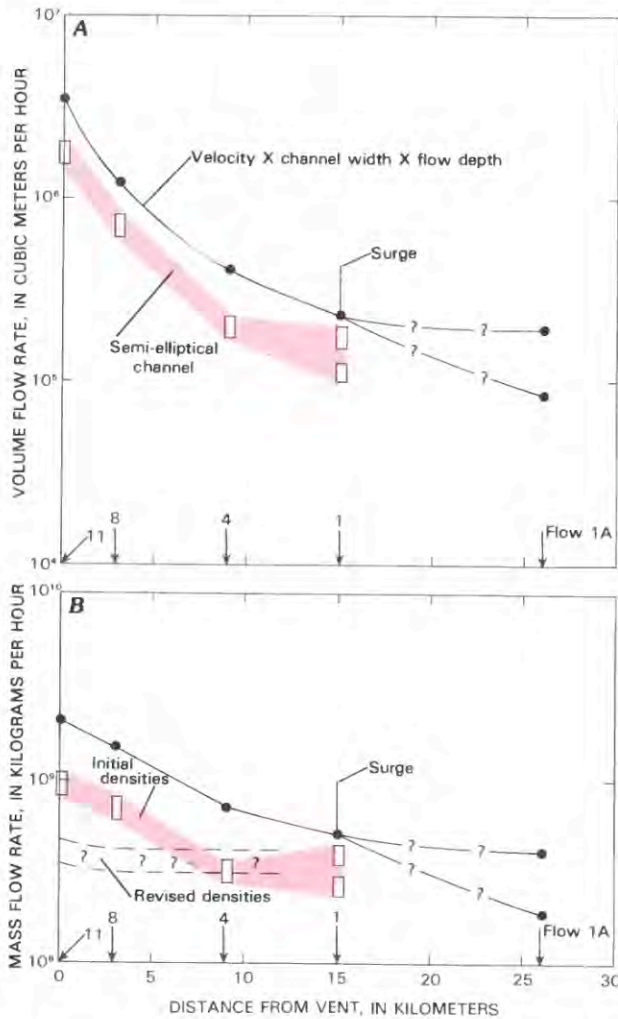


FIGURE 58.16.—Volume and mass flow rates of Mauna Loa lava on April 3, 1984. Numbers and arrows on abscissae indicate stations and their distances from the vents. Rates indicated by boxes calculated assuming semi-elliptical channels; rates indicated by dots calculated assuming rectangular flow cross sections; see text and tables 58.2, 58.3, and 58.5. **A**, Volume flow rate: note the decrease by a factor of 12 from the vent to station 1, 15 km from the vent. **B**, Mass flow rate: note the decrease by a factor near 3 from the vents to station 4, 9 km from the vent (using densities initially assumed in calculations of apparent viscosity). Band with question marks represents approximate mass flow rate calculated using revised densities that conserve mass.

0.42×10^6 m³/h at station 4, and 0.23×10^6 m³/h at station 1. Thus, volume flow rates are about 16 times larger at the vent than they are at station 1. The volume flow rates calculated for Newtonian (at the vent) and Bingham fluids in a semi-elliptical channel are 1.5×10^6 – 2.0×10^6 m³/h at the vent, 0.6×10^6 – 0.8×10^6 m³/h at station 8, 0.17×10^6 – 0.22×10^6 m³/h at station 4, and 0.10×10^6 – 0.18×10^6 m³/h for station 1. The volume flow rate

under these conditions is thus about 9 times larger at the vent than at station 4.

Mass flow rates also decrease with distance from the vent (fig. 58.16B). Mass flow rates at the vent are about 3 times larger than they are at station 4. For the rectangular flow with uniform velocity, mass flow rates are 2×10^9 kg/h at the vent and 0.7×10^9 kg/h at station 4; for reasons stated earlier these values are probably too large by a factor of about 2. For the semi-elliptical channel, mass flow rates are 0.8×10^9 – 1.1×10^9 kg/h at the vent and 0.28×10^9 – 0.37×10^9 kg/h at station 4; beyond station 4, no mass flow changes are required by the data. Thus there appears to be a mass flow of 0.5×10^9 – 0.7×10^9 kg/h that needs to be accounted for in the semi-elliptical channel calculations. This is discussed later.

DISCUSSION

APPARENT VISCOSITY

The magnitudes of the apparent viscosity calculated for the Mauna Loa lava are reasonable when compared with experimental data (Shaw, 1969). For example, graphic interpolation of instrument viscosities between 1,150 °C and 1,130–1,135 °C (Shaw, 1969, fig. 1, table 2) suggests that the viscosity of Hawaiian basalt at 1,140 °C should be near 300–400 Pa·s. This is comparable in magnitude to the viscosity calculated for lava at the vents from April 2 through the morning of April 8, which is 140–380 Pa·s. The somewhat lower values for the Mauna Loa lava may be because it was frothy; this could reduce the apparent viscosity (Shaw and others, 1968). Because maximum shear stresses decrease with time at the vents from about 1.6×10^3 Pa on April 2 through April 8 to about 500–700 Pa on April 12, the frothy lava at the vents might be expected to have apparent viscosity that increases (see, for example, Shaw and others, 1968, fig. 14). The apparent viscosity for station 8 (fig. 58.17), which is 1.1×10^3 – 1.4×10^3 Pa·s, is reasonably close to the instrument viscosity ($\sim 10^3$ Pa·s) and to the high value of the Bingham viscosity (0.75×10^3 Pa·s) measured in Makaopuhi lava at 1,130–1,135 °C (Shaw and others, 1968). Magnitudes of the apparent viscosity at stations 4 and 5 (1,920 to 1,950-m elevation) and its erratic behavior between adjacent sites and stations on the same day (fig. 58.17) might be accounted for if the lava were frothy and cooler than 1,135 °C so that it behaved somewhat like basalt at 1,125 °C and small, but variable, shear rates. Rough estimates of maximum shear stresses and shear rates for the lava at stations 4 and 5 vary within the ranges 1.8×10^3 – 3.5×10^3 Pa and 1.4 – 0.3 s⁻¹, respectively (fig. 58.17). According to Shaw (1969), instrument apparent viscosity at 1,125 °C is variable and decreases with stress up to 16×10^3 Pa and shear rates as high as 5 s⁻¹. Judging from Shaw (1969, fig. 1, inset), apparent viscosity of basalt at 1,125 °C increases from about 10×10^3 Pa·s at a shear rate of 1 s⁻¹ to about 70×10^3 Pa·s at a shear rate of 0.05 s⁻¹. Thus, if the stations 4 and 5 lava was a few degrees hotter than 1,125 °C and the bubbles affected the lava, the calculated apparent viscosities (1.9×10^3 – 12×10^3 Pa·s) are entirely reasonable. Local variations in bubble content, temperature, stress, and rate of shear could produce or contribute to the mystify-

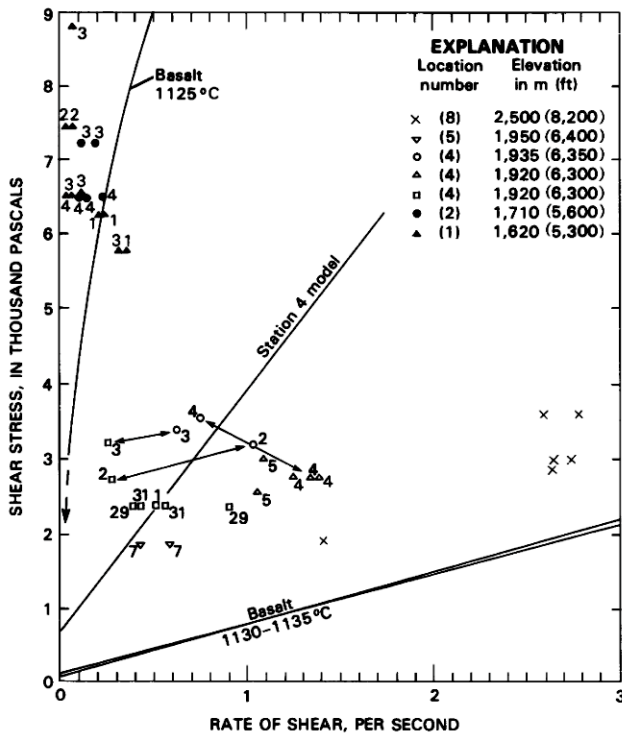


FIGURE 58.17.—Relation between approximate maximum shear stress and rate of shear for 1984 Mauna Loa lava at five stations. Lines labeled 1,130–1,135 °C correspond to data on basalt of Shaw and others (1968); curved line labeled 1,125 °C corresponds to experimental data on basalt at that temperature (Shaw, 1969). Line station 4 model is for Bingham fluid with yield strength of 680 Pa and viscosity of 3.7×10^3 Pa·s. Note that this diagram fits within inset of figure 14 of Shaw (1969) but that ordinate and abscissa are interchanged. Numbers by plotted points refer to day of month in interval March 29 to April 7; arrowed lines connect data points at different sites on the same day at station 4.

ing variations of the apparent viscosity with time and place. Increase in the volume fraction of solids in the lava, which is known to increase apparent viscosity (see, for example, Shaw, 1969; Moore and Schaber, 1975), is an added variable. For the lower reaches of the flow at stations 1 and 2, where temperatures were near 1,125 °C, maximum stress (fig. 58.17) is about 5.7×10^3 – 9×10^3 Pa, shear rate about 0.4 – 0.08 s⁻¹, and apparent viscosity 15×10^3 – 160×10^3 Pa·s. Here, the instrument apparent viscosity of approximately 10×10^3 – 70×10^3 Pa·s at 1,125 °C (see, for example, Shaw, 1969, fig. 1, inset) is in good agreement with the apparent viscosity obtained for the stations 1 and 2 lava. Apparent viscosity calculated for the toe area of flow 1A, where it must eventually reach infinity, is plausible. Walker (1967) assumes that the flow of Etna lava virtually stops when the velocity is 10^{-4} m/s and then calculates that its apparent viscosity is 10^8 – 10^{10} Pa·s. If flow 1A was advancing at a rate of 10^{-4} m/s and its thickness was unchanged, it would have an apparent viscosity of 0.4×10^9 Pa·s.

A BINGHAM LAVA

The principal reasons for considering that the Mauna Loa lava might behave as a Bingham fluid are the rheological studies of Makaopuhi lava lake (Shaw and others, 1968), observations of the flow in progress that indicate the centers of the flows move as plugs, and studies of other volcanic flows (for example, Cigolini and others, 1984). Both the yield strength and Bingham viscosity derived for the idealized station 8 at 2,500-m (8,200-ft) elevation are quite comparable in magnitude to those obtained for the Makaopuhi lava lake at similar temperatures (Shaw and others, 1968). For the lava lake, yield strength was 70–120 Pa, quite comparable to the 66–220 Pa obtained at station 8. Similarly, the Bingham viscosity for the lava lake, 0.65×10^3 – 0.75×10^3 Pa·s, is quite comparable to the 1.1×10^3 – 1.2×10^3 Pa·s obtained at station 8. For the idealized station 4, it was shown that a Bingham fluid with one set of properties could conserve mass in two adjacent sections of the same channel with different gradients and dimensions.

As noted previously, a simple Bingham model will not account for the flow at station 1. Some aspects of the model fit the observations. In particular, the upper parts of the flow moved as slabs or pluglike units. Because the model predicts that the width of the plug becomes larger than the channel, faulting and disruption of a Bingham plug into separate intact units could occur. In this case, the yield conditions could vary as a function of angle of internal friction, cohesion, and other factors (Johnson, 1970).

Parts of the Mauna Loa flow may have behaved as a Bingham fluid; but they were heterogeneous in comparison with paints and slurries. For example, the Bingham model predicts the observed slablike motion of the upper layer of wide flows and provides a mechanism for stopping the flow when it thins to its rest thickness. However, the upper slablike parts of the wide, unconfined flows are composed of blocks, clinkers, and cinders, whereas the underlying parts are composed of incandescent, molten lava. Elsewhere, the heterogeneous character of the flow is evident. At station 8, visual observations indicate the presence of the central plug required for a Bingham fluid, but the surface of the flow was clearly heterogeneous. The characteristics of the lava at depth are unknown. At lower elevations near stations 4 and 5, concentrations of fragments in the incandescent lava were larger, the fragments were darker, and the fragments were larger than at station 8; in contrast with station 8, incandescent lumps or plastic clots were evident and abundant. The flow at station 1 looked like a debris flow with warm to incandescent blocks, clinkers, and cinders, large globs or plastic clots, and local exposures of incandescent lava beneath the debris. Although the discrete, intact flow units show that the flow had some strength, and pluglike motion occurred, the Bingham model does not predict a number of intact flow units.

WHICH MODEL?

It is entirely possible that the Mauna Loa lava obeyed different flow laws at different places and times (see, for example, Shaw, 1969). The lava may have been a Newtonian fluid at the vents, a

Bingham fluid at station 8, and a pseudoplastic fluid or some other kind of fluid in the lower reaches. Concentrations of debris, incandescent blocks and fragments, and plastic clots were so large in the lower reaches of the flow on April 2 and 3 that models of the flow movements might require incorporation of concepts such as cohesion, angle of internal friction, and pore fluids.

The information necessary to establish the appropriate flow models may be embodied in existing time-lapse photography and motion pictures of the flow in progress. If satisfactory velocity profiles of the flowing lava can be obtained from the photography, they can be used to infer the rheological properties of the flow (Johnson, 1970). A velocity profile for an apparently well behaved flow confined in a leveed channel at Arenal (Cigolini and others, 1984) illustrates how such velocity profiles can be used. For the Arenal flow, the lava-filled channel was 30 m wide and 10 m deep. The slope was 30°. The central 18 m of the flow moved as a plug with a velocity of 6×10^{-3} m/s; velocity decreased from the plug to zero at the flow margins. Using the half-width of the plug and a density of $2,700 \text{ kg/m}^3$ in equation 4, the yield strength comes out to be 37×10^3 Pa, which is reasonably close to the value of 79×10^3 Pa obtained by Cigolini and others (1984) using equation 2. Equation 6 gives a Bingham viscosity of 27×10^6 Pa·s which is essentially the same as an independently measured value of 24×10^6 Pa·s for unit c of the Arenal flow at $1,075^\circ\text{C}$ (Cigolini and others, 1984).

VISCOSITY AND LAVA CHARACTERISTICS

The principal causes of the changes in viscosity and yield strength are related to changes in temperature, gas and bubble contents, concentration of solids, and plastic clots. The major changes at the vents are probably related to changes in gas and bubble contents and concentration of solids because the vent lava at $1,140^\circ\text{C}$ was frothy and had about 14–21 percent volume concentration of microphenocrysts on April 2–3; by April 13 it was still frothy and the concentration of microphenocrysts was about 27 percent (Lipman and Banks, chapter 57). A 13 percent change in microphenocryst concentration at this temperature would probably increase viscosity by a factor of 2 or so (Shaw, 1969; Moore and Schaber, 1975). Apparent viscosity of the frothy lava at the vents increased by a factor of 10 from April 2 to April 13 (fig. 58.14) with a concomitant decrease in shear stress from about 1.6×10^3 Pa to 0.5×10^3 – 0.7×10^3 Pa; it is possible that the apparent viscosity increased because the lava was also frothy (see, for example, Shaw and others, 1968, fig. 14). A similar increase could result if the lava was a Bingham or pseudoplastic fluid because both stress and rate of shear declined from April 2 to April 13.

In order to account for three orders of magnitude increase in apparent viscosity from the vent to station 1 on April 2, 3, or 4 (fig. 58.14) by microphenocrysts alone, the volume concentration would have to increase something like 20 percent (see, for example, Shaw, 1969) to 50 percent (see, for example, Moore and Schaber, 1975) above the initial 14–21 percent. The concentration of phenocrysts increased along the length of the flow, but values are not reported

(Lipman and Banks, chapter 57). Solids other than crystals that were incorporated in the lava probably contributed to the increase in apparent viscosity by analogy with slurries (Smith, 1960) and debris flows (Johnson, 1970). The fluid contained warm, solid debris, hot incandescent blocks and fragments, and molten globs or plastic clots, all set in a matrix of hotter, more fluid lava. Both the mean size and the concentrations of these objects increased along the length of the flow in a manner correlative with the increase in magnitude of the apparent viscosity. Such a correlation implies that concentrations of all kinds of objects in the flow might affect the rheology in ways analogous to the effects of solids in slurries and debris flows.

VOLUME AND MASS FLOW RATE

The conservation of mass in a complicated system such as the Mauna Loa eruption is difficult to establish because gases evolve from the lava and enter the atmosphere, lava overflows channels or becomes ponded, and there may be other sinks. In addition, the observations and data employed may contain errors. In the mass-flow calculations (fig. 58.16B), the density employed is the most likely factor that could lead to errors. In order to have a constant mass flow with volume flows of 1.5×10^6 – 2.0×10^6 m³/h through a semi-elliptical channel at the vent and roughly 0.13×10^6 – 0.16×10^6 m³/h through a semi-elliptical channel 15 km from the vent at station 1, the density of the lava must change by a factor near 12. If the density of the lava at station 1 is taken as $2,600 \text{ kg/m}^3$ (the largest value for station 1 given in Lipman and Banks, chapter 57), the density of the lava in the channel at the vent would have to be about 220 kg/m^3 instead of the 530 kg/m^3 employed in the "initial densities" mass-flow calculation (fig. 58.16B). Correspondingly changed densities for the other stations would be about 530 kg/m^3 (station 8) and $1,900 \text{ kg/m}^3$ (station 4). It is unlikely that the measured lava velocities and channel widths and the estimated flow depths could lead to a factor of 12 difference in mass flow rates between the vent and station 1 because each of these three values would have to be low by a factor of nearly 2.3 at station 1 (or high by a factor of 0.44 at the vent) or low by a factor of 1.5 at station 1 and high by a factor of 0.67 at station 11 (vent). The change in mass flow rate of 0.5×10^9 – 0.7×10^9 kg/h from the vent to station 4 on April 3 is much too large to be accounted for by the masses involved in overflows, ponding, and gas emissions.

The changes in density indicated above would reduce the apparent viscosities calculated earlier by factors of 0.4 for the vents (stations 11 and 12) and 0.5 for station 8; Bingham viscosity, most values of yield strength, and maximum stress (but not rate of shear) would be reduced by one-half for station 8. Changes for stations 4 and 1 would be less than 11 percent.

Changes in densities along the length of the flow also have implications for volume flow rates calculated from the areal extent and thickness of the lava after an eruption (Walker, 1973; Malin, 1980). For example, if the volume flow rate observed at the vent during the eruption is 2×10^6 m³/h ($560 \text{ m}^3/\text{s}$) and the density of the hot, gas-charged lava is 220 kg/m^3 , the mass flow rate is 0.44×10^9

kg/h. If the gases evolve and the lava is deposited with an average density of $2,200 \text{ kg/m}^3$, the volume flow rate would appear to be $0.2 \times 10^6 \text{ m}^3/\text{h}$ ($56 \text{ m}^3/\text{s}$), one order of magnitude smaller than the value observed at the vent. A similar conclusion is reached (Moore, 1982) when volume flow rates in channels of the 1942 Mauna Loa eruption (Macdonald, 1943; Finch and Macdonald, 1953) are compared with posteruption volume flow rates (Walker, 1973; Malin, 1980).

CONCLUSIONS

1. From April 2 to April 3, the physical appearance, behavior, and velocity of the Mauna Loa lava varied dramatically along the length of the flow. In the upper reaches, 3 km from the vents at station 8, the flow appeared to be a mass of sparse cinders and clinkers imbedded in a matrix of more fluid incandescent lava. Flow appeared to be laminar and was steady with a velocity of 5.3 m/s at the channel center. At stations 4 and 5, 9 km from the vents, the visible flow in the channel was composed of abundant dark cinders and clinkers and incandescent clots in a matrix of more fluid incandescent lava; flow was confined in channels with high levees in some places. Flow appeared to be laminar but was unsteady with small surges and ebbs. Velocity was near 1–2 m/s at the channel center. At station 1, 15 km from the vents, the flow was a hummocky mass of slowly moving debris, rubble, and blocks in a matrix of more incandescent lava confined within a rubbly leveed channel. Part of the debris and rubble and some of the blocks were incandescent but coherent. Flow appeared to be laminar but was unsteady with large surges and ebbs. Velocity varied from about 0.3 m/s during surges to about 0.1 m/s during ebbs.

2. Apparent viscosity calculated for the lava increased along the length of the flow, in parallel with physical appearance. On April 2, apparent viscosity increased from about $100 \text{ Pa}\cdot\text{s}$ at the vents to about $0.1 \times 10^6 \text{ Pa}\cdot\text{s}$, 15 km from the vents. Apparent viscosity also increased with time at the vents from about $100 \text{ Pa}\cdot\text{s}$ on April 2 to $10^3 \text{ Pa}\cdot\text{s}$ on April 12 and 13. Similar increases occurred elsewhere in the lower reaches of the flow. Like the apparent viscosity, viscosity and yield strength calculated for a Bingham fluid on April 3 increased dramatically from $10^3 \text{ Pa}\cdot\text{s}$ and $0.1 \times 10^3 \text{ Pa}$ at station 8, 3 km from the vents, to $80 \times 10^3 \text{ Pa}\cdot\text{s}$ and $2 \times 10^3 \text{ Pa}$ at station 1, 15 km from the vents. These values compare well with laboratory data on viscosity of basalt with similar temperature, stress, and shear rate. The increase in viscosity is probably related to the increase in concentration of solids and plastic clots, reduction in gas and bubble contents, decrease of temperature, and decreases in stress and shear rate.

3. The rheology of the lava probably varied along the length of the flow. It may have been a Newtonian fluid near the vents, a Bingham fluid 3 km from the vents, and a pseudoplastic fluid at larger distances from the vents. Other kinds of fluids not considered here may also apply. Existing time-lapse photography and motion pictures of the flow in progress should be reviewed and studied because they may contain information about the appropriate flow rheology.

4. Volume flow rates obtained by multiplying the maximum velocity at the channel center, the channel width, and the depth of flow are probably too large by a factor of nearly 2 because the average velocity of a flow is less than the velocity at the channel center. Mass flow rates would be affected in a similar manner. On April 3, volume flow rates at the vent were near 1.5×10^6 – $2.0 \times 10^6 \text{ m}^3/\text{h}$. Volume flow rates decreased with distance from the vents. Most of this decrease is due to increases in the density of the lava with distance from the vents. In order to approximate the conservation of mass along the length of the flow on April 3, the density of the lava flowing from the vent would have to be near 220 kg/m^3 , which implies a mass flow rate of 0.33×10^9 – $0.44 \times 10^9 \text{ kg/h}$. Lava deposited at these rates with an average density of $2,200 \text{ kg/m}^3$ would appear to have a volume flow rate of 0.15×10^6 – $0.20 \times 10^6 \text{ m}^3/\text{h}$.

REFERENCES CITED

- Bingham, E.C., 1922, *Fluidity and Plasticity*, New York, McGraw-Hill, 440 p.
- Borgia, Andrea, Linneman, Scott, Spencer, Daniel, Morales, L.D., and Andre, J.B., 1983, Dynamics of lava flow fronts, Arenal Volcano, Costa Rica: *Journal of Volcanology and Geothermal Research*, v. 19, p. 303-329.
- Caldwell, D.H., and Babbitt, H.E., 1941, Flow of muds, sludges, and suspensions in circular pipe: *Industrial and Engineering Chemistry*, v. 33, no. 2, p. 249-256.
- Cigolini, Corrado, Borgia, Andrea, and Casertano, Lorenzo, 1984, Intra-crater activity, aa-block lava, viscosity, and flow dynamics: Arenal Volcano, Costa Rica: *Journal of Volcanology and Geothermal Research*, v. 20, p. 155-176.
- Finch, R.H., and Macdonald, G.A., 1953, Hawaiian volcanoes during 1950: *U.S. Geological Survey Bulletin* 996-B, 89 p.
- Fink, J.H., Malin, M.C., D'Alli, R.E., and Greeley, Ronald, 1981, Rheological properties of mudflows associated with the spring 1980 eruptions of Mount St. Helens volcano, Washington: *Geophysical Research Letters*, v. 8, no. 1, p. 43-46.
- Hulme, Geoffrey, 1974, The interpretation of lava flow morphology: *Geophysical Journal of the Royal Astronomical Society*, v. 39, p. 361-383.
- Johnson, A.M., 1970, *Physical Processes in Geology*: San Francisco, Freeman, Cooper and Co., 577 p.
- Kilburn, C.R.J., 1981, Pahoehoe and aa lavas: discussion and continuation of the model of Peterson and Tilling: *Journal of Volcanology and Geothermal Research*, v. 11, p. 373-382.
- Krauskopf, K.B., 1948, Lava movement at Paricutin Volcano, Mexico: *Geological Society of America Bulletin*, v. 59, p. 1267-1284.
- Lockwood, J.P., Banks, N.G., English, T.T., Greenland, L.P., Jackson, D.B., Johnson, D.J., Koyanagi, R.Y., McGee, K.A., Okamura, A.T., and Rhodes, J.M., 1985, The 1984 eruption of Mauna Loa Volcano, Hawaii: *Eos, Transactions, American Geophysical Union*, v. 66, no. 16, p. 169-171.
- Lockwood, J.P., Decker, R.W., Jackson, D.B., Koyanagi, R.Y., Okamura, A.T., and Johnson, D.J., 1984a, The 1984 eruption of Mauna Loa, Hawaii: *Eos, Transactions, American Geophysical Union*, v. 65, no. 45, p. 1137.
- Lockwood, J.P., Rhodes, J.M., Garcia, Michael, Casadevall, Tom, Krueger, Arlin, and Matson, Michael, 1984b, Mauna Loa Volcano, Hawaii: *Eos, Transactions, American Geophysical Union*, v. 65, no. 18, p. 339.
- Macdonald, G.A., 1943, The 1942 eruption of Mauna Loa, Hawaii: *American Journal of Science*, v. 241, p. 241-256.
- , 1953, Pahoehoe, aa, and block lava: *American Journal of Science*, v. 251, p. 169-191.
- Malin, M.C., 1980, Lengths of Hawaiian lava flows: *Geology*, v. 8, p. 306-308.
- Moore, H.J., 1982, A geological evaluation of proposed lava diversion barriers for the NOAA Mauna Loa Observatory, Mauna Loa Volcano, Hawaii, and

- some recommendations: U.S. Geological Survey Open-File Report 82-314, 17 p.
- Moore, H.J., and Schaber, G.G., 1975, An estimate of the yield strength of the Imbrium flows: Proceedings of the Lunar Science Conference, 6th, Houston, TX, March 17-21, 1975, p. 101-118.
- Orowan, E., 1949, Remark from joint meeting of British Glaciological Society, British Rheologists' Club, and Institute of Metals: *Journal of Glaciology*, v. 1, no. 5, p. 231-240.
- Peterson, D.W., and Tilling, R.I., 1980, Transition of basaltic lava from pahoehoe to aa, Kilauea Volcano, Hawaii: field observations and key factors: *Journal of Volcanology and Geothermal Research*, v. 7, p. 271-293.
- Shaw, H.R., 1969, Rheology of basalt in the melting range: *Journal of Petrology*, v. 3, no. 3, p. 510-535.
- 1972, Viscosities of magmatic silicate liquids: an empirical method of prediction: *American Journal of Science*, v. 272, p. 870-893.
- Shaw, H.R., Wright, T.L., Peck, D.L., and Okamura, R., 1968, The viscosity of basaltic magma: an analysis of field measurements in Makaopuhi lava lake, Hawaii: *American Journal of Science*, v. 266, p. 225-264.
- Smith, R.W., 1960, Flow of limestone and clay slurries in pipelines: *Transactions, American Institute of Mining, Metallurgical, and Petroleum Engineers*, v. 217, p. 258-265.
- Sparks, R.S.J., Pinkerton, H., and Hulme, Geoffrey, 1976, Classification and formation of lava levees on Mount Etna, Sicily: *Geology*, v. 4, p. 269-271.
- Valentyik, Laszlo, 1972, Rheological properties of heavy media suspensions stabilized by polymers: *Transactions, American Institute of Mining, Metallurgical, and Petroleum Engineers*, v. 252, p. 99-105.
- Walker, G.P.L., 1967, Thickness and viscosity of Etna lavas: *Nature*, v. 213, p. 484-485.
- 1973, Lengths of lava flows: *Philosophical Transactions of the Royal Society of London, Series A.*, v. 274, p. 107-118.